



LAWRENCE
LIVERMORE
NATIONAL
LABORATORY

LLNL-JRNL-871676

Fission gas trapped in Chernobyl fuel microparticles reveals details of reactor operations

L. Leifermann, G. Balco, A. Roberts, M. Raiwa, P. Hannemann, T. Weissenborn, D. Ohm, M. Klinkenberg, M. Savina, D. van Eerten, F. Brandt, B. Isselhardt, C. Walther

December 9, 2024

Journal of Hazardous Materials

Disclaimer

This document was prepared as an account of work sponsored by an agency of the United States government. Neither the United States government nor Lawrence Livermore National Security, LLC, nor any of their employees makes any warranty, expressed or implied, or assumes any legal liability or responsibility for the accuracy, completeness, or usefulness of any information, apparatus, product, or process disclosed, or represents that its use would not infringe privately owned rights. Reference herein to any specific commercial product, process, or service by trade name, trademark, manufacturer, or otherwise does not necessarily constitute or imply its endorsement, recommendation, or favoring by the United States government or Lawrence Livermore National Security, LLC. The views and opinions of authors expressed herein do not necessarily state or reflect those of the United States government or Lawrence Livermore National Security, LLC, and shall not be used for advertising or product endorsement purposes.

1 ***Fission gas trapped in Chernobyl fuel microparticles reveals details of reactor operations***

2 Laura Leifermann¹, Greg Balco², Autumn Roberts², Manuel Raiwa², Paul Hanemann¹, Tobias
3 Weissenborn¹, David Ohm¹, Martina Klinkenberg³, Michael Savina², Darcy van Eerten¹, Felix Brandt³,
4 Brett H. Isselhardt², Clemens Walther¹

5 ¹ Institute of Radioecology and Radiation Protection, Herrenhäuserstr. 2, 30419 Hannover, Germany

6 ² Lawrence Livermore National Laboratory, Nuclear and Chemical Sciences Division, 7000 East Ave,
7 Livermore, CA 94551, USA

8 ³ IFN-2: Nuclear Waste Management, Forschungszentrum Jülich, Wilhelm-Johnen-Str., 52428 Jülich,
9 Germany

10

11

12

13

14

15

16

17

18

19

20

21

22

23

24

25 **Corresponding Author:**

26 Laura Leifermann

27 leifermann@irs.uni-hannover.de

28 +495117623069

29 Leibniz University Hannover

30 Institute of Radioecology and Radiation Protection

31 Herrenhäuserstr. 2

32 30419 Hannover

33 Germany

34 **Abstract**

35 The isotopic ratios of fission gas would provide important source information of a nuclear fuel sample
36 found in the environment. However, it is believed that during a reactor accident like Chornobyl all
37 fission gas is lost and that the radioactive particles found in the Chornobyl Exclusion Zone today are
38 depleted in gases by the initial explosion and subsequent fire. We disprove this hypothesis by detection
39 and analysis of trapped krypton and xenon in these particles. Our analysis of krypton and xenon
40 isotopes by noble gas mass spectroscopy in combination with resonance ionization mass spectrometry
41 establishes that important information about reactor operations like age, neutron flux and plutonium
42 fission fraction can still be reconstructed from individual micrometer-sized particles even after decades
43 of weathering in the environment.

44 **Keywords:** Single hot particle analysis, Noble gas spectroscopy, Chornobyl, RIMS, RBMK, FIB

45 **Environmental Implication**

46 The detection of trapped fission gases like krypton and xenon, volatile fission products, in Chornobyl
47 microparticles challenges previous assumptions that such gases were fully released at the high
48 temperatures of the accident. This new process understanding suggests that long term environmental
49 contamination by hot particles is more complex than initially thought. Understanding fission product
50 entrapment and retention in these particles - and release even after decades- highlights potential long-
51 term environmental impacts and the need for ongoing monitoring and analysis to assess ecological
52 consequences accurately of long-lived radioactive pollutants in the ecosystem.

53

54 **1 Introduction**

55 Various radioactive isotopes are released during the explosion and graphite fire at the Chornobyl
56 reactor accident in 1986. Both the United nations (UN) and the International Atomic Energy Agency
57 (IAEA) state, that this event resulted in the complete release of Krypton, (e. g. 33 PBq ^{85}Kr) and Xenon
58 (e.g. 6500 PBq ^{133}Xe) inventory of the reactor (UNSCEAR, 1988; IAEA, 2006). Additionally, fragments of
59 the nuclear fuel itself were dispersed into the environment, predominantly within the confines of the
60 Chornobyl Exclusion Zone, although the finest particles were dispersed across Europe (IAEA-Report,
61 2011). These fuel remnants, often referred to as hot particles, predominantly comprise uranium along
62 with fission and breeding products, exhibiting diverse morphologies and resilience to environmental
63 conditions (Leifermann, 2023). Most identified hot particles fall within the micrometer range
64 (Bulgakov, 2009; Salbu, 2018; Salbu, 2001; Kashparov, 2004; Kashparov, 2012; Kashparov, 2019).

65 Non-destructive analytical techniques such as Scanning Electron Microscopy (SEM), Energy Dispersive
66 Spectroscopy (EDS), and quasi-non-destructive static Secondary Ion Mass Spectrometry (SIMS),
67 Secondary Neutrals Mass Spectrometry (SNMS) and Resonant Ion Mass Spectrometry (RIMS) have
68 been essential in surface-level characterization of these particles (Raiwa, 2022a) (Bosco, 2021).
69 Furthermore, gamma measurements can be used to quantify the activity of some isotopes within the
70 particles (Leifermann, 2023). In this work, we improve upon existing characterization of particle
71 surfaces by (i) dissecting particles to reveal their unweathered internal cores, and (ii) extracting fission-
72 produced noble gases from particles as a means of diagnosing reactor operations from fission
73 products. The use of a focused ion beam (FIB) enables the examination of the unweathered internal
74 material. Approximately 15 % of all fission products generated during reactor operation manifest as
75 gaseous elements (Cassata, 2023). Notably, gases like krypton and xenon exhibit minimal solubility in
76 uranium dioxide, leading to their aggregation into bubble formations that coalesce into tunnel
77 networks within the fuel (Rest, 2019). Thus, fission gases are present both dissolved in oxide fuel at

78 the site of production and in minuscule, nanometer- to micrometer-scale bubble inclusions (Rest,
79 2019; Rest, 1989).

80 However, investigations into fission gas content of microparticles have so far been limited to spent
81 nuclear fuel particles prepared directly from research fuel samples (Cassata, 2023). The above
82 measurements have yet to be tested on environmental samples or, specifically, on hot particles from
83 Chornobyl. Important nuclear forensic information can be reconstructed by isotopic ratios from the
84 fission gases krypton and xenon. This includes information about the fuel composition and burnup,
85 neutron flux and spectrum, and the age of the sample via decay of ^{85}Kr (Balco, 2024).

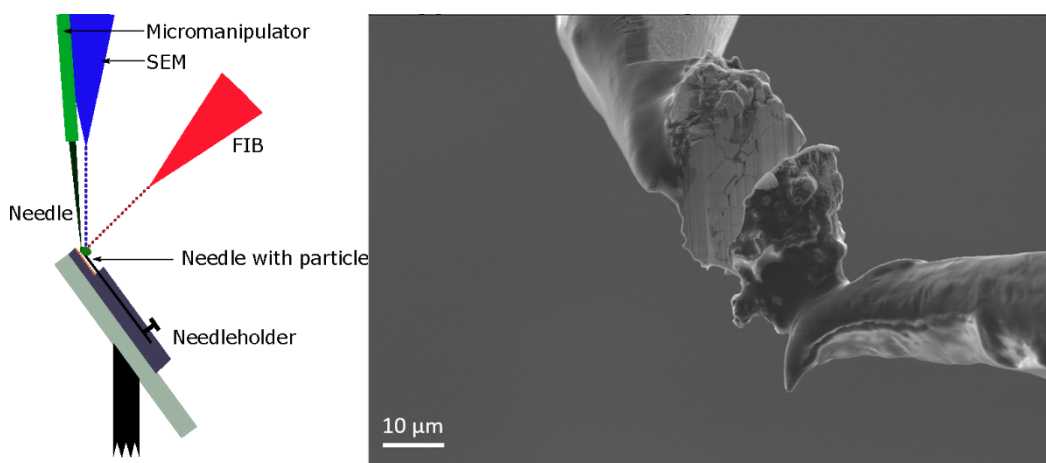
86 **2 Material and methods**

87 **2.1 Particle separation**

88 The particles described in this study were extracted from soil and sediment samples collected in the
89 Chornobyl exclusion zone in 2014 and 2017. For the analysis of particles without interfering
90 background, they must be localized in soil samples and extracted on needles. For a detailed description
91 of how this is done, refer to Leifermann et al. (Leifermann, 2023). Five particles are prepared for cutting
92 using FIB and six particles are prepared for the gas measurements.

93 **2.2 Cutting particles using focused ion beam**

94 The particle is prepared as described in Leifermann et al. so that it sticks firmly to the tip of a needle.
95 A fresh needle is mounted onto a micromanipulator (KLEINDEK NANOTECHNIK) in a focused ion beam (FIB)
96 system (NVISION 40, ZEISS) at the Researchcenter Jülich. The particle is positioned on a sample holder
97 located on the sample plate, which allowed tilting of the sample. SEMGLUE is used to attach the second
98 needle to the particle. Since this procedure has not previously been performed on particles, various
99 currents are tested and adjusted to effectively cut through the particle. Once the particle is completely
100 severed, the second needle is disengaged from the particle. Subsequently, one half of the particle is
101 retained on each needle, facilitating examination of the particle's cross-section, while the other half
102 remained available for additional measurements and analyses.



103

104 *Figure 1: Cutting process with two needles at one particle. Left: schematic diagram of the cutting process. Right: Cut particle*
105 *with one half of the particle on one needle.*

106 **2.3 Sample preparation for noble gas measurements**

107 For noble gas mass spectrometry measurements, the particles are removed from the needle tip and
108 encapsulated within a tantalum foil, which is subsequently housed within a larger tantalum enclosure
109 made by crimping a small segment of tubing (Fig. S1). This packaging is not gas-tight so that extracted
110 noble gases are released for analysis. The enclosure is then placed under vacuum and heated with a

111 140 W, 970 nm diode laser that is coupled to an optical pyrometer in a control loop that adjusts laser
112 power to achieve a specified temperature of the outer package. To prevent introduction of potential
113 hydrocarbon interferences into the mass spectrometer, each particle was initially preheated to 800° C
114 to combust the hydrocarbon glue used for particle handling, and evolved gas was pumped away
115 without analysis. Samples were subsequently heated in a series of heating steps starting at 1000° C.
116 After each heating step, evolved noble gases were purified by reaction with hot and cold getters and
117 then introduced into a Nu Instruments 'Noblesse' mass spectrometer equipped with five Faraday cup
118 detectors and five ion-counting discrete dynode multipliers. All stable xenon and krypton isotopes,
119 plus ^{85}Kr , were measured on ion multipliers. The temperature of heating steps was subsequently
120 increased in 50-100° C increments until sufficient xenon and krypton had been extracted for precise
121 isotope ratio analysis. At this point heating was halted to minimize possible damage to particles and
122 preserve them for additional analyses, so no attempt was made to quantitatively extract all fission gas
123 present. Observed Xe and Kr signals were then corrected for any atmospheric contribution by assuming
124 that all ^{80}Kr and ^{129}Xe observed are atmospheric, and correcting other isotope signals according to their
125 atmospheric ratios. In most cases atmospheric corrections were less than 5% for major isotopes.
126 Finally, amounts of Xe and Kr isotopes released in all heating steps for each sample were summed to
127 calculate mean isotope ratios for all fission gas released from that sample. The complete step-
128 degassing data are reported in table S5 in the supplementary material.

129

130 **2.4 RIMS measurements after noble gas measurements**

131 Following the measurements, the particle must be localized again. This is achieved by carefully
132 unfolding the foil and applying a very dilute sugar solution onto it. The approximate position of the
133 particle is continuously monitored using a Geiger Müller Counter (GMC). Subsequently, the foil is
134 inserted into a SEM to precisely locate the particles on the surface. The particle can then be further
135 analyzed using RIMS at Lawrence Livermore National Laboratory (LLNL). For the analysis of zirconium
136 as well as uranium and plutonium, the methodologies are described by Raiwa et al. and van Eerten et
137 al. (Raiwa, 2024; van Eerten, 2023).

138 **3 Results**

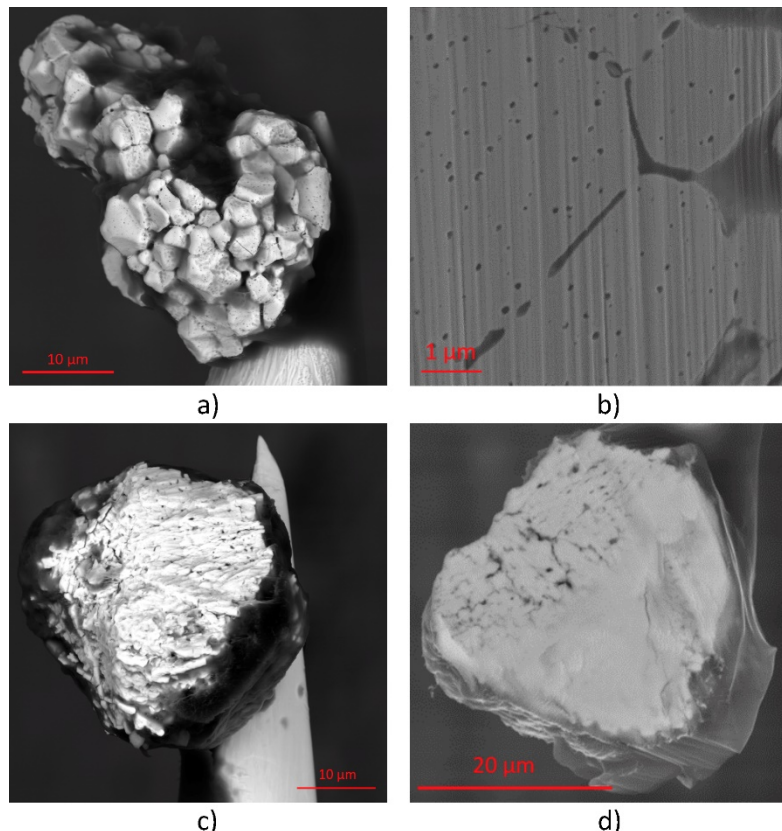
139 In this work, five particles are successfully cut using FIB and six particles are analyzed using noble gas
140 mass spectrometry. The particles are labeled with names. An overview of the gamma activities of the
141 with noble gas mass spectrometry analyzed particles can be found in table 1.

142 *Table 1 The table shows the particles measured using noble gas mass spectrometry. The activity is given in Bq at the time of*
143 *measurement. The morphology estimated from the structure in the SEM image and the main elements measured in the EDS*
144 *are also shown. It is evident that the particles exhibit adhesions of various elements on their surface, including Fe and S. The*
145 *nomenclature of the particles is employed for the purpose of identification.*

Particle	Date of Measurement	^{137}Cs [Bq]	^{241}Am [Bq]	Main elements	Morphology
Ares	18 th March 2019	150(1)	7.6(1)	U, Zr, Fe	$\text{U}_x\text{Zr}_y\text{O}_z$
Eurybia	20 th January 2023	19.2(1)	0.82(1)	U	UO_2
Heimdall	03 th August 2021	10.1(1)	0.51(1)	U	-
Ida	04 th August 2021	0.09(1)	1.0(2)	U, Fe, S	UO_2
Nereus	12 th August 2022	28.8(1)	1.68(2)	U	UO_{2+x}
Thor	17 th August 2022	19.3(1)	1.36(2)	U	UO_2

146

147 While EDS measurements of particles' surfaces reveal features like molten zirconium from the fuels
148 cladding, no such inhomogeneous features on the micrometer size were observed within the particles
149 (Fig. S2 Supplement). The important feature shown in the SEM images in figure 2 is the intact pore
150 structure that permeates the entire particle regardless of the apparent surface structure. The pores
151 and grain boundaries are both sealed and isolated from one another, preventing the escape of any gas.
152 Due to the small size of these gas bubbles, they are only evident on smooth surfaces which necessitates
153 the FIB cut. This pore structure spanning from a few micrometers down to the nanometer scale is the
154 result of the produced fission gases during reactor operation. Such voids are commonly encountered
155 in spent nuclear fuel and grow with higher burnup (Rest, 2019).



156
157 *Figure 2: a) Particle structure of Momos before cutting. b) Pore structure of Momos after cutting with FIB c) Particle Mjöllnir
158 with weathering before cutting, d) Pore structure of weathered particle Mjöllnir*

159

160 **3.1 Noble gas measurements**

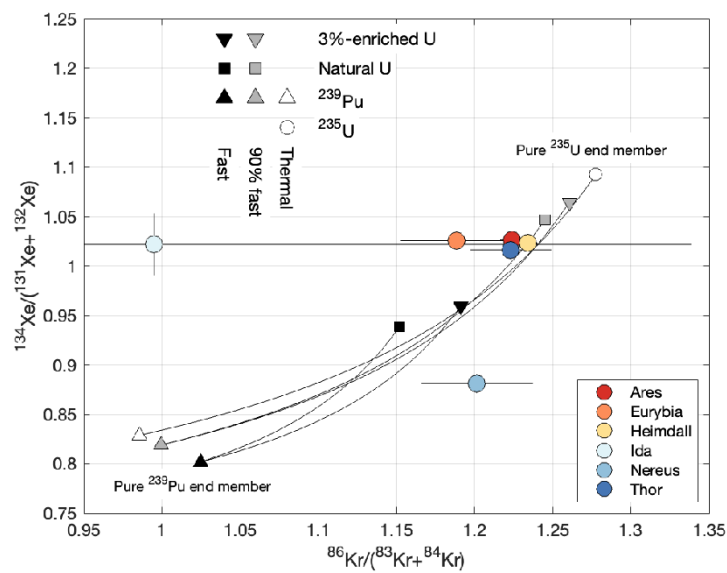
161 As the temperature in the reactor core at meltdown is estimated at 2500 °C, the presence of fission
162 gas released by heating to the 1000° - 1200 °C range indicates that the analyzed particles must have
163 been ejected from the reactor well before peak core temperatures were reached. However, the
164 presence of zirconium coatings on some particles that contain noble gases indicates at least brief
165 exposure to temperatures at or above the melting point of Zr (1800 °C) (Kashparov, 2012) (Devell,
166 1986). The presence of noble gases in these particles indicates that they are not readily released from
167 oxide fuels, even in extreme conditions of fire, explosion, and exposure to environmental weathering
168 over long periods of time.

169 Particles without a Zr-cladding are also released. The Zr-cladding of the Ares particle, for example, may
170 be interpreted as part of the molten cladding material, consisting of a zirconium alloy, and thus of
171 natural isotope ratios. It cannot be ruled out that the uranium itself was not exposed to such high

172 temperatures and that the Zr only melted on top of it. The measured particles were probably not
 173 exposed to the high temperatures in the reactor, as it would not have been possible to measure
 174 krypton, xenon and cesium under such conditions. The presence of burnup dependent fissionogenic Zr
 175 can be discerned in all particles, wherein this element is integrated into the particle's structural
 176 composition. Nevertheless, the surface of the particle may also exhibit Zr originating from the Zr
 177 utilized in the cladding. Substantial quantities of gas are detected even within particles lacking visible
 178 surface pores. This finding validates statements made by Rest et al. (Rest, 2019) regarding the
 179 nanometer-scale size of these pores, which may be less discernible on rough surfaces. Consequently,
 180 these measurements confirm that the bubbles observed in the cut particles contain fission gas.
 181 However, it has no environmental consequences because, firstly, the gas is safely trapped in the fuel,
 182 secondly, large parts of it have already decayed in the fuel itself. Thirdly, even if it were released, the
 183 high radioactivity is in the xenon radioisotopes, which decayed a long time ago due to its short half-life
 184 and the remaining noble gases are inert and have only little effect on human body.

185 3.2.1 Source

186 Analysis of the isotope ratios of xenon and krypton can clarify the specific parent isotopes that
 187 underwent nuclear fission due to the different thermal fission yields for ^{235}U and ^{239}Pu . The ratio
 188 $^{86}\text{Kr}/(^{83}\text{Kr}+^{84}\text{Kr})$ is used because $^{83}\text{Kr}+^{84}\text{Kr}$ is insensitive to neutron capture after production and thus
 189 reflects the fission yield ratio rather than the neutron flux (Balco, 2024). The ratio $^{134}\text{Xe}/(^{131}\text{Xe}+^{132}\text{Xe})$
 190 adheres to analogous principles. Notably, these fission yield ratios exhibit significant divergence
 191 between uranium and plutonium fission, this makes them valuable for isotopic characterization.
 192 (Cassata, 2023; Balco, 2024). The different fission yields for Pu-fission of ^{86}Kr (0.761) and $^{83}\text{Kr}+^{84}\text{Kr}$
 193 (0.484+0.294) result in a ratio of one for pure Pu fission. If there is more U fission, the fission yield for
 194 ^{86}Kr (1.96) increases much more than for $^{83}\text{Kr}+^{84}\text{Kr}$ (0.996+0.552) and the ratio shifts to 1.3 (Magill,
 195 2018). The same assumptions and justifications of $^{86}\text{Kr}/(^{83}\text{Kr}+^{84}\text{Kr})$ also apply to $^{134}\text{Xe}/(^{131}\text{Xe}+^{132}\text{Xe})$.
 196 With the fission yields for ^{235}U , the ratio of $^{134}\text{Xe}/(^{131}\text{Xe}+^{132}\text{Xe})$ for pure uranium fission is 1.07 and for
 197 ^{239}Pu with a pure plutonium fission is the ratio 0.75.



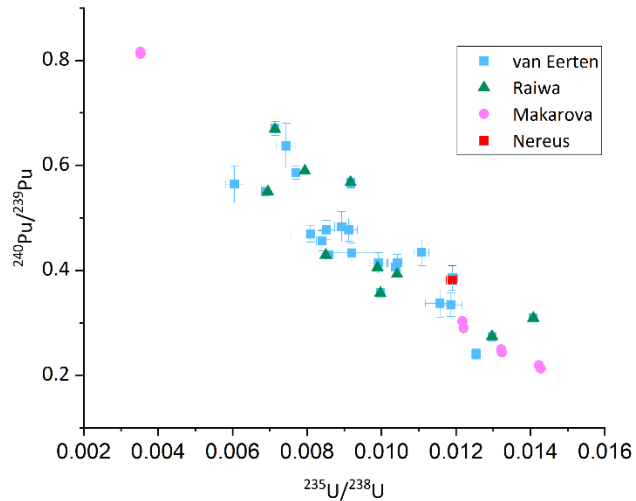
198

199 Figure 3: The plotted $^{86}\text{Kr}/(^{83}\text{Kr}+^{84}\text{Kr})$ to $^{134}\text{Xe}/(^{131}\text{Xe}+^{132}\text{Xe})$ ratios serve as indicators of the likely sources of these isotopes
 200 from nuclear fission processes. Reference lines corresponding to the variation of the initial ratios during production in a range
 201 of fission sources on the figure for comparison (Balco, 2024). The extremities of calculated values are highlighted using gray
 202 and black triangles and boxes, delineating the range of possible ratios. Each colored dot on the plot represents a measured
 203 ratio of $^{86}\text{Kr}/(^{83}\text{Kr}+^{84}\text{Kr})$ to $^{134}\text{Xe}/(^{131}\text{Xe}+^{132}\text{Xe})$, providing empirical data points within the context of the plotted theoretical
 204 calculations.

205 In four of the measured particles (Ares, Eurybia, Heimdall, Thor) in fig. 4 the resulting fission gases are
 206 mainly caused by uranium fission. This also fits very well with the fuel used in the reactor, which has
 207 an enrichment level of approximately 2 % ^{235}U and a low burnup of around 11 GWd/tU (GRS, 1987,
 208 USSR, 1986) (Kashparov, 2018) (Wakabayashi, 1987). The substantial error bars observed for Ida stem
 209 from the limited gas release during these measurements which is consistent with its small size, low
 210 ^{137}Cs concentration, and the likelihood of variable loss of included fission gas during ejection in the
 211 explosion. Consequently, it is unsurprising that the recorded gas quantities are modest, resulting in
 212 high uncertainties.

213 The isotopic composition of the Nereus particle deviates significantly from that of the other
 214 microparticles. This is far outside the expected range and indicates significantly more ^{239}Pu fission in
 215 the production of the fission gases. Both, the krypton and the xenon ratios are in the range of more
 216 plutonium fission, although the xenon values differ more.

217 The SIMS and SNMS results suggest that the isotope ratios U and Pu of Nereus are not unusual. They
 218 are exactly in line with the trend of the particles measured in various previous studies by van Eerten
 219 (van Eerten, 2023) and Raiwa (Raiwa, 2022b) and the data published by Makarova et al. (Makarova, et
 220 al., 2008). The particle is in the medium burnup range.

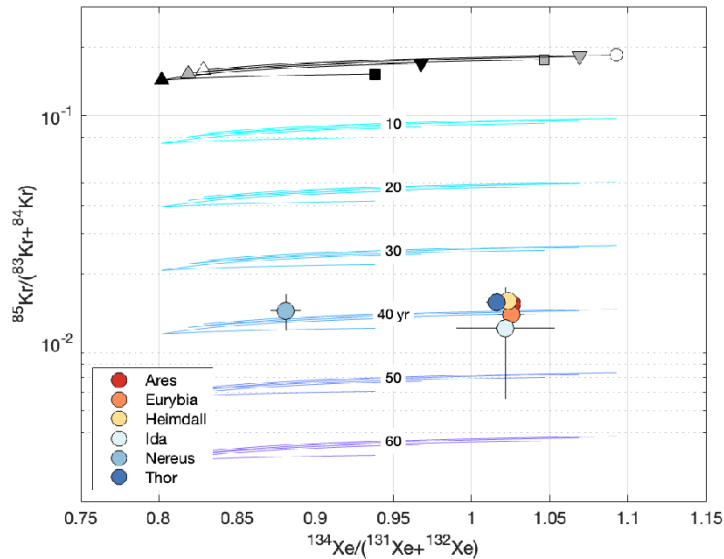


221

222 Figure 4 The isotope ratios of $^{235}\text{U}/^{238}\text{U}$ and $^{240}\text{Pu}/^{239}\text{Pu}$ were measured with RIMS and SNMS. The data from van Eerten et al.
 223 (van Eerten, 2023) and Raiwa (Raiwa, 2022b) and Makarova et al. (Makarova, et al., 2008) were used. Nereus lies exactly in
 224 the trend of the particles and is not an outlier. The particle has an average burn-up and the U and Pu values provide no
 225 indication of a particle that was formed from other fuels.

226 3.2.2 Age Dating

227 Figure 5 indicates how the date when the particles were irradiated can be inferred from the Kr and Xe
 228 isotope composition. The initial $^{85}\text{Kr}/(^{83}\text{Kr}+^{84}\text{Kr})$ ratio varies somewhat with the fissioning material, but
 229 can be estimated by its correlation with the stable isotope ratios $^{134}\text{Xe}/(^{131}\text{Xe}+^{132}\text{Xe})$ or $^{86}\text{Kr}/(^{83}\text{Kr}+^{84}\text{Kr})$,
 230 which are also diagnostic of the fission source. Measured $^{85}\text{Kr}/(^{83}\text{Kr}+^{84}\text{Kr})$ ratios are much less than
 231 estimated initial ratios due to radioactive decay, which allows an estimate of the date of irradiation.
 232 All particles have indistinguishable ^{85}Kr dates ranging from October, 1981 +/- 8 years to November,
 233 1985 +/- 1 year, with a median age of July, 1985. This is consistent with the typical residence time of
 234 Chornobyl fuel rods in the reactor was 1100-1200 days (Bibilashvili, Yu K., F. G. Reshetnikov, A. G.
 235 Ioltukhovsky, 1998).



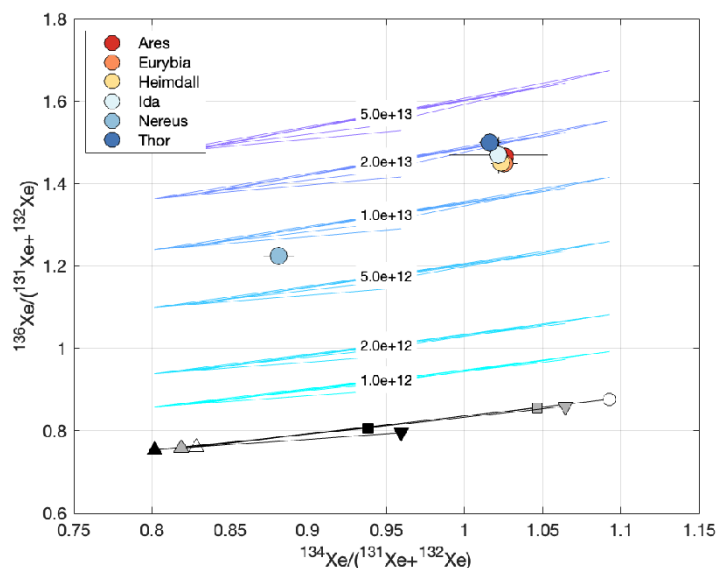
236

237 *Figure 5: The age of the particles is shown in the figure. The source of the fission is again indicated on the X-axis. The ratio of*
 238 *the radioactive ^{85}Kr ($T_{1/2}=10,74$ years) to the stable $^{83}\text{Kr}+^{84}\text{Kr}$ is given on the Y-axis. From this, the age of the particles can be*
 239 *easily calculated using the decay law. The black lines give the fission yields, which is the initial isotope ratio at formation, for*
 240 *various fission sources, with the same color-coding as in Figure 4. The colored dots are the measured particles. The horizontal*
 241 *lines indicate the different decades to which the isotope ratios can be calculated back. All particles are calculated to have a*
 242 *similar age of approximately 40 years. The position of Nereus shows again that it must come from a different source of fission*
 243 *than the other particles.*

244

3.2.3 Thermal neutron Flux Densities

245 Isotope ratios involving ^{136}Xe can be used to estimate thermal neutron flux densities in the reactor.
 246 ^{136}Xe is produced through neutron capture by ^{135}Xe , which boasts a notably high thermal neutron
 247 capture cross-section of 2.65×10^6 b. The conversion of ^{135}Xe to ^{136}Xe scales with the thermal neutron
 248 flux density. This relationship underscores the utility of ^{136}Xe as a sensitive indicator of neutron activity
 249 under varying operational conditions. The values for all particles except Nereus are usual for the RBMK
 250 reactor and correspond to the expected values (Gulshani, 1987; Ohm, 2023). Noticeable different is
 251 the Nereus particle with significantly lower values for the thermal neutron flux densities.



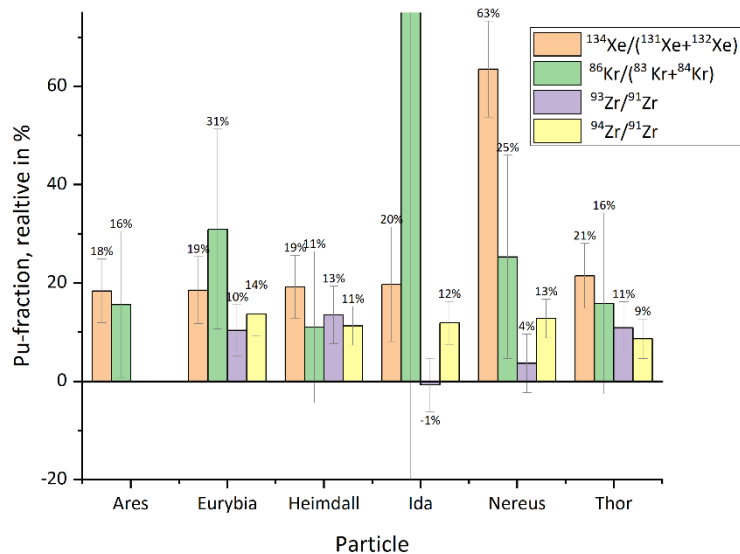
252

253 *Figure 6 The Xe isotope ratios are plotted on the X-axis, as in fig. 4, which indicate the source of the fission gases. The Y-axis*
 254 *shows the ^{136}Xe isotope ratios, which are normalized to the same isotopes as for ^{134}Xe . The ^{136}Xe is an indicator of the thermal*

255 neutron flux densities in the reactor. The black lines give the fission yields, which is the initial isotope ratio at formation, for
 256 various fission sources, with the same color-coding as in Figure 4. while horizontal lines represent various calculated thermal
 257 neutron flux densities, compare to fig. 4. The majority of data points cluster around the $2 \times 10^{13} \text{ cm}^{-2} \text{ s}^{-1}$ range, which is relatively
 258 low but characteristic of RBMK reactors. Nereus exhibits a distinct deviation from other particles, indicating significantly lower
 259 thermal neutron flux exposure compared to the rest of the dataset.

260 3.3 Comparison with RIMS Measurements

261 The isotopic ratios of zirconium were also measured by resonance ionization mass spectrometry
 262 (RIMS). The Zr originates from two different sources: Zirconium produced by fission (fissiogenic) is
 263 incorporated into the U matrix and distributed homogeneously over the particles' entire UO_2 matrix.
 264 Natural Zr is used for the fuel cladding. Hence, Zr at the surface of the particles has natural isotope
 265 ratios and little or no fissiogenic zirconium isotopes. Analogous to the noble gas measurements the
 266 different fission yields are used to estimate the fraction of ^{239}Pu fissions. The method is described in
 267 detail by Raiwa et al. (Raiwa, 2024). In brief, the $^{93}\text{Zr}/^{91}\text{Zr}$ and $^{94}\text{Zr}/^{91}\text{Zr}$ ratios shift from 1.10 and 1.09
 268 for 100% ^{235}U fission towards 1.6 and 1.77 with increasing ^{239}Pu fissions respectively. Interference from
 269 non-fissiogenic zirconium is ruled out by comparing the results of both isotope pairs. In this case the
 270 $^{93}\text{Zr}/^{91}\text{Zr}$ would drop as ^{93}Zr is pure anthropogenic and not found in natural zirconium while the ratio
 271 of $^{94}\text{Zr}/^{91}\text{Zr}$ shifts towards its natural abundance ratio of 1.55. These shifts lead to a discrepancy in the
 272 calculated ^{239}Pu fission fraction which indicate contamination with natural zirconium. In this study this
 273 was the case for the particle Ares which clearly shows cladding fused to its surface (Fig S3.).



274

275 Figure 7: The isotope ratios of $^{86}\text{Kr}/(^{83}\text{Kr}+^{84}\text{Kr})$ and $^{134}\text{Xe}/(^{131}\text{Xe}+^{132}\text{Xe})$ as well as of fissiogenic $^{93}\text{Zr}/^{91}\text{Zr}$ and $^{94}\text{Zr}/^{91}\text{Zr}$ are shown.
 276 The fissiogenic Zr is built into the UO_2 matrix of the particles in contrast to the Zr cladding from the fuel rods. The proportion
 277 of ^{239}Pu fission is calculated from these ratios and plotted on the y-axis for the respective isotope ratios and particles. No Zr
 278 ratios could be measured for Ares, as it has a Zr cladding with natural Zr isotope ratios. The fissiogenic Zr was measured for
 279 the other 5 particles. The error bars for Ida are particularly large, as hardly any gas could be measured here.

280 The results for the remaining five particles are given in fig. 7. All particles show about 10 % fission
 281 fraction from ^{239}Pu which is comparable to the calculated value by the noble gas measurements (For
 282 $^{134}\text{Xe}/(^{131}\text{Xe}+^{132}\text{Xe})$ all particles around 20%, but Nereus 63%, $^{86}\text{Kr}/(^{83}\text{Kr}+^{84}\text{Kr})$ more differences between
 283 the particles from 11% to 31% and Ida, which is not evaluable with the large uncertainties). One particle
 284 (Ida) shows a lower fission fraction consistent with 0 for the ^{93}Zr based value. As the value is outside
 285 the 1-sigma uncertainty of the ^{94}Zr value this is most likely a result of a minor natural zirconium

286 interference. Nereus shows smaller spots of zirconium, which could be cladding material with neutral
287 zirconium isotopic ratios in the element mapping, which can also reduce the apparent $^{93}\text{Zr}/^{91}\text{Zr}$ ratio.

288

289 **4 Discussion**

290 Analysis of the cut edges has provided deeper insights into the nature of fuel fragments from
291 Chornobyl, particularly highlighting the presence of gas inclusions within the particles regardless of
292 surface structure and environmental weathering. The predominant closed porosity of the particles
293 results in the retention of the gas. The gas inclusions in the particles can originate from the detected
294 pores or be incorporated into the UO_2 matrix. These particles contain significant amounts of noble
295 gases that persist decades after the Chornobyl accident which is in direct disagreement with previous
296 reports where it was stated that all fission gas was lost from the core (UNSCEAR, 1988).

297 Plutonium is generated over time within a reactor through neutron capture by uranium and
298 subsequent decay processes. This transformation results in the formation of plutonium with typically
299 small quantities within the reactor. A review of the data from the noble gas measurements reveals
300 that, with one exception, the data agree on their assessment of the fuel burnup, origin, thermal
301 neutron flux, etc. The sole particle that fails to meet expectations is Nereus. There is no evidence that
302 plutonium was contained as a raw material in the Chornobyl reactor (GRS, 1987, USSR, 1986, GRS,
303 1996). It can be definitively stated that mixed oxide fuel (MOX) was not used in the Chornobyl incident,
304 as the U and Pu isotope ratios of Nereus are clearly consistent with those observed in Chornobyl and
305 the other measured particles (Dawahrah, 1991). At the top and bottom ends of the fuel rod, the
306 neutron fluxes are significantly lower than in the middle of the fuel rod. In addition, the neutron flux
307 densities decrease from the outside to the inside of the reactor, so an additional factor here could be
308 not only the upper edge of the fuel rod, but also the radial center of the reactor. The higher $^{132}\text{Xe}/^{131}\text{Xe}$
309 ratio of Nereus indicates a that the particle experienced more fluence and thus a longer time in the
310 reactor. So, on the one hand we have the values of ^{134}Xe , which indicate a high burnup, and on the
311 other hand the ratio of $^{136}\text{Xe}/(^{131}\text{Xe}+^{132}\text{Xe})$, which indicates a low neutron flux, thus low burnup and a
312 longer time in the reactor. Also, the $^{235}\text{U}/^{238}\text{U}$ ratios of 1.22 % indicate, that this particle has a very low
313 neutron flux. A prolonged residence time and/or an edge position in a relatively low neutron flux region
314 of the reactor can account for the majority of the observations.

315 The possibility of an adherent contamination of Xe can be excluded, because negligible ^{129}Xe was
316 observed. The ^{129}Xe is the indicator for contamination with atmospheric xenon, since this is not formed
317 in the reactor due to the long half-life of the parent nuclide ^{129}I ($T_{1/2}=1.57*10^7$ years) (Magill, et al.,
318 2018). The origin of the Xe isotope ratios is evident for all particles, with the exception of Nereus, for
319 which a definitive explanation remains elusive.

320 The measured isotope ratios and the calculated age of the particles are consistent with the literature
321 on the Chornobyl reactor accident (UNSCEAR, 1988) (Makarova, et al., 2008). There is no radiological
322 hazard from the noble gases that have not yet been released or are being released slowly. The
323 calculated age of the particles clearly dates them into the irradiation period before the accident. It is
324 unnecessary to determine the age of the particles from Chornobyl, as the release period is known.
325 However, determining the age of other radioactive particles of unknown origin or from several sources
326 is beneficial for further research. While such a radiochronology analyses is also possible by the isotopic
327 pair $^{90}\text{Sr}/^{88}\text{Sr}$ (van Eerten, 2023; Savina, 2023) this gives an important second measurement, which
328 were done for Ares and Heimdall by van Eerten et al. (van Eerten, 2023) and calculates to be $1985 \pm$
329 1, therefore the same age as the ^{85}Kr measurements for these two particles. Here the produced fission
330 gas is partially lost during the irradiation period while the strontium does not suffer from this effect

331 (Balco, 2023). There is no radiological hazard from the up to 1.5% of noble gases in particles in the
332 environment that have not yet been released or are being released slowly. 98,5% of the original
333 inventory in Chornobyl remained in the shelter. The correct identification of a sample from the edge
334 of a pellet is of paramount importance in nuclear forensics as its elemental and isotopic ratios differ
335 dramatically from the average fuel pellet and thus would lead to wrong conclusions about the source
336 of the sample (Desgranges, 2009; Walker, 2009). The results after heating the particles give the same
337 results and were thus confirmed by two different measuring devices RIMS and SNMS before and after
338 heating. This validation underscores the reliability and robustness of the analytical approach employed
339 in this study.

340 **5 Conclusion**

341 In summary, the measurements conducted have yielded significant success. Two novel methods for
342 analyzing particles originating from Chornobyl have been established and will be utilized in future
343 studies. The process of cutting the particles has been proven effective, enabling one half of them to
344 serve as reference materials for future measurements. Analysis of the cut edges has provided deeper
345 insights into the nature of fuel fragments from Chornobyl, particularly highlighting the presence of gas
346 inclusions within the particles. Noble gas measurements carried out at LLNL have opened up new
347 possibilities for studying μ m-sized particles. These particles contain significant amounts of noble gases
348 that persist decades after the Chornobyl accident. These measurements made it possible to identify
349 whether the particles came from fission processes of uranium or plutonium. What is impressive is that
350 the age of the particles could be determined to a specific time window before the accident happened,
351 despite the small amounts of gas measured. Furthermore, reconstruction of thermal neutron flux
352 densities within the reactor during operation is achieved based on these measurements. They are
353 aligning well with calculated models. Additionally, RIMS measurements conducted post-heating of the
354 particles to high temperatures have consistently provided results corroborated by two separate
355 measurement devices. This validation underscores the reliability and robustness of the analytical
356 approach employed in this study.

357 **6 Outlook**

358 Further studies on more particles from Chornobyl and on Nereus would help to unravel the puzzle of
359 the unusual Xenon isotope ratios. It would also be interesting to investigate other particles with
360 unusual isotope ratios to see if there could be more samples with possibly more Pu fission.

361 The noble gas measurements can also be carried out in the future on other sources. These
362 measurements could explain the origin and history of unknown fuel samples. Other types of reactors
363 should have different characteristic gas releases and should also be distinguishable from detonated
364 nuclear weapons. Furthermore, more particles from Chornobyl should be examined in order to be able
365 to better explain particles like Nereus and to increase the statistics.

366 **7 Acknowledgements**

367 Many thanks to Murat Güngör for his lab work at FIB at Research center Jülich.

368 Part of this work was performed under the auspices of the U.S. Department of Energy by Lawrence
369 Livermore National Laboratory under Contract DE-AC52-07NA27344. This is LLNL-JRNL-871676.

370 Many thanks for the financial support from the Siebold-Sasse-Foundation, the SOLARIS project BMBF
371 2020+ 02NUK075A and the LISA project.

372 **8 References**

373 Balco, G., Conant, A. J., Reilly, D. D., Barton, D., Willett, C. D., and Isselhardt, B. H. 2024. Krypton-85
374 chronometry of spent nuclear fuel. *Geochronology Discuss.* [preprint]. 2024.

375 Bibilashvili, Yu K., F. G. Reshetnikov, A. G. Ioltukhovsky. 1998. Status and development of RBMK fuel
376 rods and reactor materials. 1998.

377 Bosco, H., Hamann, L., Kneip, N., Raiwa, M., Weiss, M., Wendt, K., Walther, C. 2021. New horizons in
378 microparticle forensics: Actinide imaging and detection of ^{238}Pu and ^{242}mAm in hot particles.
379 *Science advances.* 2021, Vol. 7, 44, p. eabj1175.

380 Bulgakov, A., Konoplev, A., Smith, J., Laptev, G., Voitsekhovich, O. 2009. Fuel particles in the
381 Chernobyl cooling pond: current state and prediction for remediation options. *Journal of*
382 *environmental radioactivity.* 2009, Vol. 100, 4, pp. 329–332.

383 Cassata, W. S., Isselhardt, B. H., Conant, A. J., Charboneau, J., Carney, K. P. 2023. Noble gas
384 constraints on spent fuel irradiation histories. *Journal of Radioanalytical and Nuclear Chemistry.*
385 2023, Vol. 332, 8, pp. 3151–3159.

386 Dawahrah, S. 1991. Increasing Plutonium Disposition Rate in the Thermal Reactors (VVER AND RBMK).
387 Vienna: IAEA, 1991. p. 552. 0074-1884.

388 Desgranges, L., Pasquet, B., Valot, Ch., Roure, I. 2009. SIMS characterisation of actinide isotopes in
389 irradiated nuclear fuel. *Journal of Nuclear Materials.* 2009, Vol. 385, 1, pp. 99–102.

390 Devell, L., Tovedal, H., Bergström, U., Appelgreen, A., Chyssler, J., Andersson, L. 1986. Initial
391 observations of fallout from the reactor accident at Chernobyl. *Letters to nature.* 1986, Vol. 321, pp.
392 192–193.

393 Gesellschaft für Reaktorsicherheit (GRS) mbH. Neue Erkenntnisse zum Unfall im Kernkraftwerk
394 Tschernobyl. 1987. GRS-S-40

395 Gesellschaft für Reaktorsicherheit (GRS) mbH. Tschernobyl-Zehn Jahre danach. 1996. GRS - 121 Köln :
396 s.n. p. 186.

397 Gulshani, P., Dastur, A. R. and Chexal, B. 1987. Stability analysis of spatial power distribution of the
398 RBMK-100 reactor. *Transactions of the American Nuclear Society.* 1987, pp. 383–386.

399 IAEA. 2006. Environmental consequences of the Chernobyl accident and their remediation: twenty
400 years of experience. 2006, STI PUB 1239.

401 IAEA-Report. 2011. Radioactive Particles in the Environment: Sources, Particle Characterization and
402 Analytical Techniques. Vienna: s.n., 2011. 978-92-0-119010-9.

403 Kashparov, V. A., Ahamdach, N., Zvarich, S. I., Yoschenko, V. I., Maloshtan, I. M., Dewiere, L. 2004.
404 Kinetics of dissolution of Chernobyl fuel particles in soil in natural conditions. *Journal of*
405 *environmental radioactivity.* 2004, Vol. 72, 3, pp. 335–353.

406 Kashparov, V., Levchuk, S., Zhurba, M., Protsak, V., Khomutinin, Y. et.al. 2018. Spatial datasets of
407 radionuclide contamination in the Ukrainian Chernobyl Exclusion Zone. *Earth System Science Data.*
408 2018, Vol. 10, pp. 339-353.

409 Kashparov, V., Salbu, B., Levchuk, S., Protsak, V., Maloshtan, I., Simonucci, C., Courbet, C., Nguyen, H.,
410 Sanzharova, N., Zabrotsky, V. 2019. Environmental behaviour of radioactive particles from Chernobyl.
411 *Journal of environmental radioactivity.* 2019, Vols. 208-209, p. 106025.

412 Kashparov, V., Yoschenko, V., Levchuk, S., Bugai, D., van Meir, N., Simonucci, C., Martin-Garin, A. 2012.
413 Radionuclide migration in the experimental polygon of the Red Forest waste site in the Chernobyl
414 zone – Part 1: Characterization of the waste trench, fuel particle transformation processes in soils,
415 biogenic fluxes and effects on biota. *Applied Geochemistry*. 2012, Vol. 27, 7, pp. 1348–1358.

416 Leifermann, L., Weiss, M., Chyzhevskyi, I., Dubchak, S., Hanemann, P., Raiwa, M., Schulz, W.,
417 Steinhauser, G., Weissenborn, T., Walther, C. 2023. Localisation, isolation and leaching of single hot
418 particles from various environmental matrices in the vicinity of the Chernobyl nuclear power plant.
419 [book auth.] Nicholas Evans. *Environmental Radiochemical Analysis VII*. 1st ed. La Vergne : RSC, 2023,
420 pp. 1–18.

421 Magill, J., Pfennig, G. and Galy, J. 2018. *Karlsruher Nuklidkarte*. 10. Auflage. Karlsruhe; Lage :
422 Nucleonica GmbH; Marktdienste Haberbeck GmbH, 2018. p. 72. 9783943868500.

423 Makarova, T. P., Bibichev, B. A. and Domkin, V. D. 2008. Destructive analysis of the nuclide
424 composition of spent fuel of WWER-440, WWER-1000, and RBMK-1000 reactors. *Radiochemistry*. 50,
425 2008, pp. 414–426.

426 Ohm, D. 2023. Berechnung isotopischer Fingerprints verschiedener Reaktortypen für die nukleare
427 Forensik. Leibniz University Hannover : IRS, 2023.

428 Raiwa, M. 2022b. Zerstörungsfreie Analyse von Kernbrennstoffpartikeln aus der Sperrzone
429 Tscherbonyls. s.l. : Hannover : Institutionelles Repozitorium der Leibniz Universität Hannover, 2022.

430 Raiwa, M., Büchner, S., Kneip, N., Weiß, M., Hanemann, P., Fraatz, P., Heller, M., Bosco, H., Weber, F.,
431 Wendt, K., Walther, C. 2022a. Actinide imaging in environmental hot particles from Chernobyl by
432 rapid spatially resolved resonant laser secondary neutral mass spectrometry. *Spectrochimica Acta*
433 Part B: Atomic Spectroscopy. 2022, Vol. 190, p. 106377.

434 Raiwa, M., Savina, M., Shulaker, D. S., Roberts, A., Isselhardt, B. 2024. Zirconium analysis in
435 microscopic spent nuclear fuel samples by resonance ionization mass spectrometry. *JAAS*. 2024.

436 Rest, J. 1989. Validation of mechanistic models for gas precipitation in solids during postirradiation
437 annealing experiments. *Journal of Nuclear Materials*. 1989, 168, pp. 243–261.

438 Rest, J., Cooper, M.W.D., Spino, J., Turnbull, J. A., van Uffelen, P., Walkrt, C. T. 2019. Fission gas
439 release from UO₂ nuclear fuel: A review. *Journal of Nuclear Materials*. 2019, Vol. 513, pp. 310–345.

440 Salbu, B., Kashparov, V., Lind, O., Garcia-Tenorio, R., Johansen, M., Child, D., Roos, P., Sancho, C.
441 2018. Challenges associated with the behaviour of radioactive particles in the environment. *Journal*
442 of environmental radioactivity. 2018, Vol. 186, pp. 101–115.

443 Salbu, B., Krekling, T., Lind, O. C., Oughton, D. H., Drakopoulos, M., Simionovici, A., Snigireva, I.,
444 Snigirev, A., Weitkamp, T., Adams, F., Janssens, K., Kashparov, V. A. 2001. High energy X-ray
445 microscopy for characterisation of fuel particles. *Nuclear Instruments and Methods in Physics*
446 Research Section A: Accelerators, Spectrometers, Detectors and Associated Equipment. 2001, Vols.
447 467–468, pp. 1249–1252.

448 Savina, M. R., Shulaker, D., Isselhardt, B., Brennecke, G. 2023. Rapid isotopic analysis of uranium,
449 plutonium, and americium in post-detonation debris simulants by RIMS. *Journal of Analytical Atomic*
450 *Spectrometry*. 2023, Vol. 38, 6, pp. 1205–1212.

451 UNSCEAR. 1988. *UNSCEAR 1988 Report*. [ed.] United Nations Scientific Committee on the Effects of
452 Atomic Radiation. 1988. p. 647.

453 USSR and Energy, State Committee on the Utilization of Atomic. 1986. The Accident at the Chernobyl
454 Nuclear Power Plant and its Consequences. Vienna : s.n., 1986. p. 532.

455 van Eerten, D., Raiwa, M., Hanemann, P., Leifermann, L., Weissenborn, T., Schulz, W., Weiß, M.,
456 Shulaker, D., Boone, P., Willingham, D., Thomas, K., Sammis, B., Isselhardt, B., Savina, M., Walther, C.
457 2023. Multi-element isotopic analysis of hot particles from Chornobyl. Journal of hazardous
458 materials. 2023, Vol. 452, p. 131338.

459 Wakabayashi, T., Mochizuki, H., Kitahara, T. 1987. Analysis of Chernobyl Reactor Accident (I). s.l. :
460 Nuclear Engineering and Design 103, 1987.

461 Walker, C. T., Bremier, S., Portier, S., Hasnaoui, R., Goll, W. 2009. SIMS analysis of an UO₂ fuel
462 irradiated at low temperature to 65MWd/kgHM. Journal of Nuclear Materials. 2009, Vol. 393, 2, pp.
463 212–223.

464

465 Energy Dispersive Spectroscopy (EDS)

466 Focused ion beam (FIB)

467 International Atomic Energy Agency (IAEA)

468 Resonant Ion Mass Spectrometry (RIMS)

469 Scanning Electron Microscopy (SEM)

470 Secondary Ion Mass Spectrometry (SIMS)

471 Secondary Neutrals Mass Spectrometry (SNMS)

472 United nations (UN)

473